# Segmental Dynamics of Solid-State Poly(methylphenylsilane) by 1D and 2D Deuterium NMR

**Robert D. O'Connor,[†] Frank D. Blum,*[,†,‡] Eric Ginsburg,[‡,§] and Robert D. Miller[‡]**

*Department of Chemistry and Materials Research Center, University of Missouri—Rolla, Rolla, Missouri 65409-0010, IBM Research Division, IBM Almaden Research Center, San Jose, California 95120-6099, and Abbott Laboratories, 97D/AP4, Abbott Park, Illinois 60064-3500*

*Received February 3, 1998; Revised Manuscript Received May 26, 1998*

ABSTRACT: The segmental dynamics of solid-state poly(methylphenylsilane) were probed with deuterium solid-echo and two-dimensional exchange (2D-X) NMR via a methyl-$d_3$ label. Between 25 and 50 °C, the spectra indicated that the polymer consisted of two fractions—a fast fraction with correlation times ($\tau_c$) below $10^{-5}$ s and one with $\tau_c$'s above 10 s. Above 50 °C, motion with $\tau_c$'s around $10^{-3}$ s was also detected. A minimization routine was developed to fit the 2D-X spectra to a model of isotropic rotational diffusion with a distribution of $\tau_c$'s. The best fits were obtained with trimodal stretched-exponential distributions. The trimodal distributions consisted of a fast mode with $\tau_c$'s around $10^{-5}$ s, an intermediate mode with $\tau_c$'s between $10^{-4}$ and 0.3 s, and a slow mode with $\tau_c$'s generally above 10 s. As the temperature increased from 56 to 90 °C, the fast fraction steadily increased from 21% to 50% while its average $\tau_c$ remained around $10^{-5}$ s; the intermediate fraction remained relatively constant at 23% while its average $\tau_c$ decreased from 125 to 8 ms, and the rigid fraction decreased from 55% to 32% with an average $\tau_c$ around 40 s. The fast fraction was attributed to amorphous segments, the rigid fraction to crystalline segments, and the intermediate fraction to segments that formed an interphase between the two.

## Introduction

Poly(methylphenylsilane) (PMPS) is a relatively new polymer.[1] Its $\sigma$-delocalized Si−Si bonds, $\pi-\pi$ interactions, and thermal and chemical stability give it unique characteristics. It has potential in microlithography, nonlinear optics, electrical conduction, and photoconduction, as an initiator in free radical polymerization, and as a polymer modifier via either blending or copolymerization.[2−10]

The microscopic properties of PMPS such as morphology, molecular order, dynamics, their interdependence, and their dependence on chemical structure form a basis for understanding its properties. The local structure, solid-state morphology, and electronic structure of PMPS have been investigated with liquid-state NMR, X-ray diffraction, UV spectroscopy, conformational energy calculations, and thermal analysis. Liquid-state $^{29}$Si NMR showed that PMPS polymerized with Na consisted of long runs of iso- and syndiotactic sequences.[10] Other polymerization methods produced a more random polymer, or the results were unknown.[11,12] X-ray diffraction studies suggested that PMPS contained multiple crystalline phases, though it was primarily amorphous.[10,13] Molecular mechanics calculations revealed that both tacticities strongly preferred the trans conformation.[14] This preference led to extended, rodlike chains and also influenced the UV absorption of PMPS.[2,10] A thermal analysis study showed that the PMPS was stable to 290 °C and had two transition regions, both mildly dependent on molecular mass.[13] The first region was broad, spanning 60 °C, and was assigned to the glass transition ($T_g$). Its midpoint shifted from 90 to 120 °C as the molecular mass increased from 28 500 to 653 000 Da. The second region started between 150 and 200 °C, depending on molecular mass, and ended at 250 °C, apparently independent of mass. It was assigned to a premelt, phase-disordering transition.

Many macroscopic properties such as moduli, thermal transitions, viscosity, heat capacity, dielectric relaxations, charge transport, and even surface adhesion have been correlated with the dynamics of polymer systems.[15−20] For example, the $T_g$ of a polymer is generally regarded as occurring at the onset of backbone motion, and the α- and $\beta$-relaxations have been related to segmental and side group dynamics, respectively.[20−22] Though the varying morphologies, tacticities, packing, and connectivities complicate the characterization of polymer dynamics, the dynamics of PMPS can be simply divided into fast-rotating methyl groups, slower-rotating phenyl groups, and backbone reorientations. In this paper, we report on the segmental dynamics of solid-state high molecular mass PMPS. Using a methyl-$d_3$ label and deuterium NMR, we incorporate results from solid-echo, relaxation, and two-dimensional exchange (2D-X) NMR experiments to describe the segmental dynamics of PMPS.

## NMR Background

Solid-state deuterium NMR is based on the quadrupolar interaction that makes the NMR frequency, $\omega$, of a deuteron dependent on the angle between its bond vector and the external magnetic field. For a methyl deuteron that reorients rapidly about its symmetry axis and has a cylindrically symmetric electric-field gradient, this relation is well approximated by[23−25]

$$\omega = \pm(3/16)(2\pi e^2 qQ/h)(3\cos^2\phi - 1)(3\cos^2\theta - 1) \quad (1)$$

where $\phi$ is the angle between the bond vector and symmetry axis, 70.5°, $\theta$ is the angle between the symmetry axis and external magnetic field, and $e^2qQ/h$

* To whom correspondence should be sent at the University of Missouri—Rolla. E-mail: fblum@umr.edu.
† University of Missouri—Rolla.
‡ IBM Research Division.
§ Abbott Laboratories.

S0024-9297(98)00149-1 CCC: $15.00 
Published on Web 07/09/1998

is the quadrupole coupling constant, QCC, which is 160−170 kHz for a typical methyl deuteron.[24] To be considered rapid, the correlation time, $\tau_c$, of the reorientation must be much faster than the reciprocal of the QCC. The rapid motion of a methyl deuteron around its symmetry axis reduces the resonance width by one-third or from about 250 to 82 kHz, compressing the signal and, consequently, increasing the S/N ratio. Also, as a result of the rotation, $\theta$ becomes the angle monitored, and a methyl group becomes a direct probe for segmental reorientations. Finally, the rotation reduces the spin−lattice relaxation time, $T_1$, allowing faster scan repetitions. Unfortunately, the smaller $T_1$'s also limit the time scales of exchange experiments.

Deuterium NMR spectroscopy has many advantages for dynamics studies in both liquids and solids.[25−27] One of its main advantages is its extremely wide dynamic range. Roughly 10 orders of magnitude in reorientation rates can be probed through different experiments.[20−28] Another advantage is the variety of experiments available for investigating different aspects of a system such as rates, geometry, distances, etc.[17,20−30] Deuterium 2D-X NMR can reveal both the time scale and geometry of reorientations with $\tau_c$'s above about 1 ms—the slow and ultraslow motion typical of polymer backbones in the solid state. Faster motion can also be studied, but interpreting the 2D-X spectra is more complicated.[31]

Spiess et al.[31−34] have described the pulse sequence and information content of the 2D-X experiment in detail. Essentially, the experiment consists of three time periods: evolution, $t_1$; mixing, $t_m$; detection, $t_2$. The evolution and detection periods are typically much smaller than the mixing period and serve to correlate reorientations occurring during the mixing period. In the slow-motion limit where $\tau_c > 1$ ms, the experiment correlates a bond vector's angle to the magnetic field before and after the mixing period. After appropriate processing, the resulting 2D-X spectrum represents the joint probability of having frequency $\omega_1$ initially and frequency $\omega_2$ at $t_m$ seconds later—the frequency being related to the angle through eq 1. The spectrum is a direct map of Markov motion, i.e., reorientations that do not depend only on their preceding positions. Motional models are, in principle, not required to interpret the spectra. Higher dimensional exchange experiments can even map non-Markovian dynamics.[24]

In general, a 2D-X spectrum shows the geometry and the relative amount of the motion occurring during $t_m$. The diagonal intensity represents the fraction of bond vectors that were either static or returned to their original position, and the off-diagonal intensity is from bonds that changed their orientation. This information can be summarized in a one-dimensional reorientation angle distribution (RAD).[24] A RAD shows the fraction of bond vectors that reoriented a specific number, $\beta$, of degrees. The values of $\beta$ range from 0 to 90° with angles greater than 90° folding over to $180° - \beta$ because of the $\cos^2$ dependence of $\theta$. RAD's can be calculated from spectra by several methods.[24,35] For a discrete jump of $\beta$ degrees during $t_m$, the off-diagonal intensity forms ellipses in the 2D plane and intensity at $\beta$ or $180° - \beta$ in the RAD. Other dynamics have different off-diagonal intensity profiles and RAD's.

A series of 2D-X experiments with different $t_m$'s can show how the exchange changes with time. In fact, a series of spectra at different $t_m$'s is representative of a correlation function.[24] Thus, the geometry, $\tau_c$, and general time evolution of the dynamics can be found from a series of 2D-X spectra with different mixing times.

Unfortunately, the above description of 2D-X NMR applies to the slow-motion limit where motion occurs only during mixing. If the $\tau_c$'s are in the intermediate region ($10^{-6} < \tau_c < 10^{-4}$ s), the accompanying frequency changes that occur during $t_1$ and $t_2$ can cause spectral distortion as compared to slow-motion spectra, a loss of the direct angle-frequency relation (eq 1) and, if a refocusing pulse is used (as is typical), strong intensity reductions.[31,35] The spectra no longer represent simple two-time joint probabilities. They depend on the type of motion occurring during $t_1$ and $t_2$. Consequently, interpreting spectra are more complicated and RAD's cannot be extracted without additional information. Similar to line-shape analysis, information can still be deduced from these intermediate 2D-X spectra by comparison with simulations based on motional models. In brief, motion during $t_1$ and $t_2$ can be taken into account if a model is introduced. But, unlike the slow-motion limit, model independent extraction of geometric and time-scale information is not possible without additional information.

The distributions of motional rates that are common in polymer systems also complicate the analysis of 2D-X specta.[36,37] If the distribution has little intensity in the intermediate region, the amount of reorientation occurring can still be extracted and summarized in RAD's. Often, however, both the shape of the distribution and the reorientation mechanism cannot be simultaneously deduced. Higher-dimensional exchange experiments or other data can help determine or limit the mechanism and distribution.[20,38,39] Typically, though, polymer dynamics are quantified by assuming a model and distribution consistent with the exchange (and possibly other data) and the parameters chosen to adequately reproduce experimental spectra. A more systematic and perhaps more accurate procedure might be to fit the parameters of a model to a series of exchange spectra with different $t_m$'s with a minimization algorithm. We developed such a routine to analyze the 2D-X spectra of PMPS. Our minimization program accounts for the intensity loss of the intermediate region and incorporates other data to further constrain the parameters. Also, a relatively straightforward addition to the program is suggested that would account for the changes in both the spectra and intensity that occur in the intermediate region.

## Experimental Section

Chlorophenylsilane was prepared as described by Schidbaur.[40] Dissolved in THF and in an argon atmosphere at 0 °C, it was converted to phenyltrideuteriomethylsilane ($PhCD_3H_2Si$) through a Grignard reaction with $CD_3MgI$. By refluxing for 27 h at 80 °C in an argon atmosphere with $CCl_4$ and $Pt^{II}Cl_2$, the $PhCD_3H_2Si$ was chlorinated to dichlorophenyltrideuteriomethylsilane ($Cl_2PhCD_3Si$). Finally, in toluene at 65 °C, $Cl_2PhCD_3Si$ was polymerized with Na to poly(trideuteriomethylphenylsilane) (PMPS-$d_3$). It was precipitated and fractionated with methanol.[9,41] The GPC trace was *unimodal* with molecular mass and polydispersity equal to 426 000 Da and 2.3, respectively, based on polystyrene standards.

Differential scanning calorimetry was run on a TA Instruments DSC model 2010 at a rate of 3 °C/min from −100 to +300 °C with an 8 mg sample.

NMR experiments were done at 61.3 MHz on a Varian VXR-S spectrometer with an Oxford 400 89 mm magnet. A fixed frequency 8 mm probe (Doty Scientific, Columbia, SC)

with a 90° pulse width, calibrated at each temperature, of 2.7 $\mu$s was used. An Oxford VTC4 unit regulated the temperature to ±1 °C with an absolute calibration of ±2 °C. Samples were first heated to 110 °C and then cooled to the desired temperature. The quadrupole-echo pulse sequence, eq 2, was used for the 1D spectra.[42]

$$\pi/2_x-\tau-\pi/2_y-\tau-\text{FID (echo)} \quad (2)$$

For these spectra, roughly 2k scans were accumulated at a repetition rate of 2 s using a 2 MHz sweep width, $\tau = 30$ $\mu$s, eight phase-cycles, 8k points zero filled to 16k, and 1 kHz Gaussian line broadening. A five-pulse sequence, eqs 3a and 3b, with 128 phase-cycles was used for the 2D-X spectra.[34] The echo delays, $\tau_1$ and $\tau_2$, were set to 2 and 25 $\mu$s, respectively.

$$\cos \pi/2-\tau_1-\pi/2-\tau_1-t_1-\pi/2-t_m-\pi/2-\tau_2-\pi/2-\tau_2-t_2 \quad (3a)$$

$$\sin \pi/2-\tau_1-\pi/2-\tau_1-t_1-\pi/4-t_m-\pi/4-\tau_2-\pi/2-\tau_2-t_2 \quad (3b)$$

The repetition rate was 1.75 s, which was about 4 times the longest $T_1$, giving essentially completely relaxed spectra. Hypercomplex data sets with 32−64 $t_1$ increments, 256−512 $t_2$ points, and 512−2 048 scans were scaled and Fourier transformed as described in ref 43. Both dimensions had 200 kHz sweep widths and 5 kHz Gaussian broadening and were zero filled to 512 points before the transform. The 2D-X pulse sequence in the sine mode with the same parameters except for a 2 MHz sweep width in $t_2$ and $t_1 = 17$ $\mu$s was used to collect spin alignment, $T_{1Q}$, spectra. The relatively low S/N of the spectra was a consequence of having only about 20 mg of PMPS-$d_3$.

Because the 2D spectra were more susceptible to experimental errors, the spectral intensities were measured by integrating the solid-echo spectra. The probe response was checked with poly(α-methylstyrene)-$d_3$ from −25 to +100 °C. Only a Boltzmann distribution temperature correction was required. The amount of isotropic species was estimated by fitting a theoretical static spectra (variable QCC and line broadening) to the experimental solid-echo powder pattern and subtracting.

The experimental spectra were prepared for the minimization routine by first removing any baseline or offset and scaling them so that $^3/_4$ QCC equaled 1. Then, the points within $\omega_{1,2} = \pm 1$ (the points containing the 2D-X spectra) were interpolated to a grid with a surface fitting routine and symmetrized according to

$$S(\omega_1,\omega_2) = S(\omega_1,\omega_2) + S(-\omega_1,-\omega_2) + S(\omega_2,\omega_1) + S(-\omega_2,-\omega_1) \quad (4)$$

i.e., across the diagonal and antidiagonal ($C_{2v}$ symmetry). $S(\omega_1,\omega_2)$ represents a 2D-X spectra with reduced frequency coordinates $\omega_1$ and $\omega_2$. Approximately 9000 points from the triangular region enclosed by the diagonal, antidiagonal, and the line $\omega_1 = 1$ were taken from the grid and used in the minimization routine. Points with $\omega_1$ less than 0.1 (8 kHz) and greater than 0.95 (38 kHz) were excluded because of the isotropic signal and low S/N ratio, respectively. These data and their corresponding theoretical subspectra points (discussed below) were then normalized. Diagonal fractions were measured by fitting a similarly prepared experimental diagonal spectrum ($T = 22$ °C, $t_m = 1$ ms) to the spectra.

Single-jump-angle spectra or subspectra were calculated in the frequency domain as described by Schmidt-Rohr et al.[24] They were calculated in 2° increments and convoluted with 1 kHz Gaussians in both dimensions. At smaller Gaussian widths, the minimization procedures discussed below did not fit the singularities of the diagonal or antidiagonal well. At larger widths (>1.5 kHz) the fitting routine converged to different points depending on the initial guess. The subspectra were linearly independent without Gaussian convolution;[35] i.e., the 40° subspectra could not be reproduced with combinations of the 38° and 42° (or any other) subspectra. We suspected that they lost this quality to varying degrees with convolution, resulting in multiple minima for the fitting routine and a large dependence on the initial guess.

As a consistency check to the main, model-constrained minimization program, RAD's free from any constraints imposed by a model were generated from experimental spectra by fitting a superposition of single jump-angle spectra to the experimental spectra.[35] For these *experimental* or *free* fit RAD's, the parameters were the weight of each theoretical subspectra from 0° to 90° in 2° increments (45 variables).

The main minimization program used a Levenberg−Marquardt nonlinear minimization algorithm to optimize the parameters of a model to reproduce a series of experimental spectra with different $t_m$'s.[46] The model was that of isotropic rotational diffusion (IRD) with a distribution of $\tau_c$'s. The distribution was heterogeneous, which means that spatially different regions of the sample had different $\tau_c$'s. Starting with an initial guess of the parameters and a series of spectra, the constrained fitting procedure consisted of calculating a discrete distribution of $\tau_c$'s, which consisted of 80 logarithmically spaced points; generating a new distribution by weighting this distribution with each $\tau_c$'s spectral intensity and renormalizing; generating a composite RAD for each $t_m$ in the series as a sum, weighted by this new distribution, of the RAD's for each $\tau_c$ in the distribution; calculating theoretical spectra as a sum of single-jump-angle subspectra weighted by the composite RAD's, and evaluating their fit to the experimental spectra. Points with an error outside of two standard deviations from the average error were excluded.[47] New parameters were then calculated by the search algorithm and the process was repeated until an optimal solution was reached. As mentioned previously, RAD's are only applicable to slow-motion spectra; so, $\tau_c$'s less than $10^{-4}$ s were ignored in the calculation of composite RAD's. However, to partially account for $\tau_c$'s in the intermediate region and faster, the procedure allowed only distributions that reproduced the spectral intensity and fast-isotropic fraction (central resonance) of the solid-echo spectra. The theoretical fast-isotropic fraction was taken as the intensity with $\tau_c$'s $< 3 \times 10^{-6}$ s. The intermediate region could have been further defined by constraining the distribution to reproduce the intensity losses from several solid-echo experiments with different delay times. Alternatively, interpolations, similar to those discussed below, from previously simulated intermediate-region spectra could have been used to directly incorporate the spectral changes of the intermediate region into the minimization routine. Neither of these efforts were required for the PMPS-$d_3$ data, though.

It should also be noted that both the RAD's and intensities were calculated prior to the minimization procedure. For a specific $\tau_c$ (or $\tau_c/t_m$ for the RAD's), the RAD was calculated analogously to the calculation of ref 32 and, the theoretical intensity was taken as the $t_2 = 0$ point of the cosine data set calculated similarly to the simulations below, except with the parameters of the solid-echo sequence, i.e., $\tau_1 = 30$ $\mu$s and $t_m = \tau_2 = t_1 = 0$. From these calculations, 80 RAD's and intensity values, logarithmically spaced in $\tau_c$ (or $\tau_c/t_m$), were splined together with a shape-preserving routine. The actual values used in the minimization were interpolations from these splines. These interpolations made the minimization very efficient.

With multimodal distributions, the minimization routine was biased to favor the smallest $\tau_m$ and narrowest width for the fast fraction that fit the intensity and isotropic resonance. For the trimodal distributions, the exchanging and static parameters were fitted first. Then, the intensity and isotropic constraints were introduced and all of the parameters were allowed to vary. In addition, for the trimodal fits, the initial guess for the $\tau_m$ of the static fraction was 75 s. This parameter changed little if the guess was above 25 s. Only the width and weight of this mode seemed relevant, indicating that its most important attributes were its weight relative to the exchanging fraction and its small $\tau_c$ tail, as would be expected from the $t_m$'s used.

Simulated spectra could have been taken directly from the fitting routine. Like the fits, though, these would only have

included the intensity reduction of the intermediate region and not the actual spectral changes that result from motion during $t_1$ and $t_2$. Thus, as a check on this approximation, simulations based on the parameters of the fit that accounted for motion during $t_1$ and $t_2$ were generated as described by Kaufmann et al.[34] These simulations calculated time-domain data sets using IMSL numerical routines, 180 × 180 matrices, double precision, and no recursion relations. The addition of the first echo ($\tau_1$) to the pulse sequence resulted in a small modification of eq 30 in ref 34. The resulting equation was

$$G_{\pm}(t_1,t_2,\tau_1,\tau_2,t_m) = \langle 1|(\tilde{P}^s_{1|0})^{1/2}\,\tilde{Q}_{s\pm}(t_2)\,\tilde{Q}_{s\pm}(\tau_2)\,\tilde{Q}_{s-}(\tau_2)\times \tilde{K}_s(t_m)\,\tilde{Q}_{s+}(t_1)\,\tilde{Q}_{s+}(\tau_1)\,\tilde{Q}_{s-}(\tau_1)\,(\tilde{P}^s_{1|0})^{1/2}|1\rangle \quad (5)$$

where the terms are the same as defined in ref 34. The calculations of the exchange and equilibrium matrices for the IRD model were similar to those of ref 32. The data sets for each $\tau_c$ in the distribution were then weighted by the distribution, summed, and processed the same as the experimental data. The effect of an angle-independent (homogeneous) spin−spin, $T_2$, of 450 $\mu$s was included in the calculations. The effects of $T_1$ and $T_{1Q}$ relaxation were not explicitly considered; but, to mimic the decay of the signals during $t_m$, the intensities of the fast ($\tau_c < 10^{-5}$ s) and slow ($\tau_c > 10^{-5}$ s) time-domain data were weighted with an effective $T_1 = T_{1Q} = 100$ ms and $T_1 = T_{1Q} = 400$ ms, respectively. These values were based on the $T_1$ values measured at 90 °C for the isotropic resonance at 0 Hz and the 90° orientation at around ±20 kHz. The measured values for $T_1$ and $T_{1Q}$ of the other isochromats were, at most, 25% smaller than those used. Including this angular dependence of the relaxation would only have significantly affected experiments with $t_m$'s longer than about 400 ms.

To facilitate convergence, the distribution corresponding to a stretched exponential correlation function[44] (SE distribution) was multiplied by a Gaussian. Its discrete, unnormalized form was

$$f(t) = \sum_{k=0}^{\infty}(-1)^{k+1}\frac{\Gamma(1+k\alpha)}{k!}(\tau/\tau_m)^{k\alpha}\sin(\pi k\alpha)e^{-(\tau/\tau_m)^2} \quad (6)$$

where $\tau$ was the correlation time; $\tau_m$ was a scaling parameter, essentially the distribution maximum; α was a width parameter ($0 < \alpha < 1$), corresponding to the exponent in the correlation function; and, Γ was the gamma function. Without the modification, narrow distributions behaved erratically above $\tau_m$. Other approximations[45] to the distribution had similar problems.

A skewed distribution, less complex than the SE, was created by applying a similar modification to the log-normal distribution. Denoted as the single-sided log-normal distribution (SSLN), its discrete, unnormalized form was

$$f(\tau) = e^{-(\ln(\tau/\tau_m)/\sigma)^2}e^{-(\tau/\tau_m)^2} \quad (7)$$

Again, $\tau$ was the correlation time; $\tau_m$ was a scaling parameter, also the distribution maximum; and, $\sigma$ was a width parameter ($0 < \sigma$). It had the same basic shape as the SE, but without as long a tail toward short correlation times.

## Results

The solid-echo spectra of PMPS from 10 to 90 °C are shown in Figure 1. Except for a central resonance that increased in intensity as the temperature increased, the spectra were typical of a deuterated methyl group rapidly reorienting about its symmetry axis. The central resonance (referred to as the *fast-isotropic* fraction) was from methyl groups that reoriented relatively isotropically with $\tau_c$'s less than about $10^{-6}$ s. The splitting of the powder pattern decreased from 41 kHz at 10 °C to 39 kHz at 90 °C. Spectra below 10 °C (not shown) did not differ in form from the 10 °C spectrum. Figure 2 shows the Boltzmann-corrected intensities

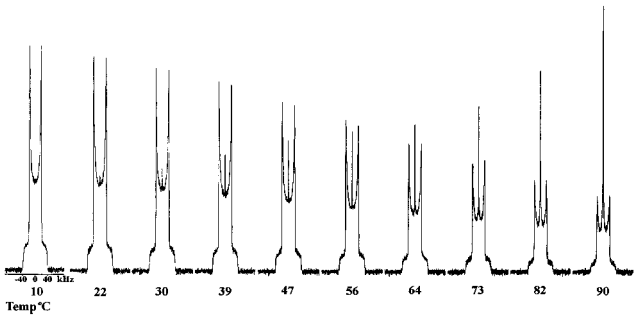


**Figure 1.** Fully relaxed solid-echo spectra of PMPS-$d_3$ with $\tau = 30$ $\mu$s. The spectra are scaled only by their number of scans (absolute intensity mode).

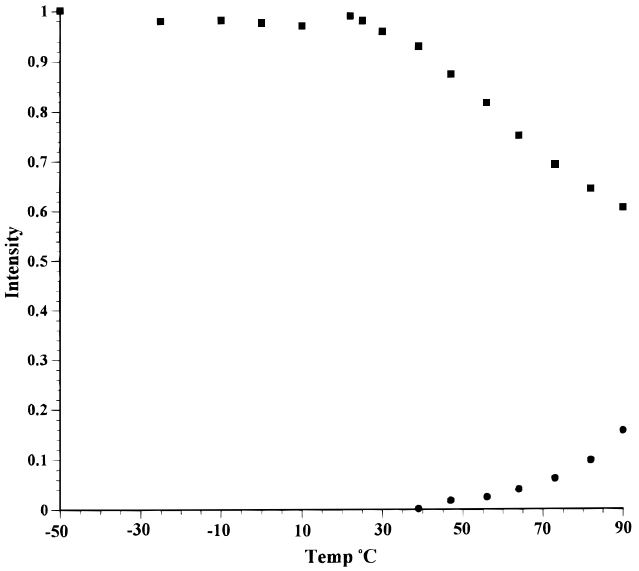


**Figure 2.** Boltzmann-corrected spectral intensity (■) and fast-isotropic fraction (●) as a function of temperature, measured from the quadrupole-echo spectra of PMPS-$d_3$.

relative to the −50 °C spectra and the fast-isotropic fractions of these spectra. In general, the spectra consisted of both rigid and mobile fractions with the rigid fraction decreasing and the mobile fraction increasing as the temperature increased. In addition, the intensity loss compared to the fast-isotropic fraction indicated that most of the mobile material was in the intermediate region and only a small part was visible as a fast-isotropic resonance.

Spin alignment, $T_{1Q}$ relaxation spectra at 56 °C with varying delay (mixing) times are shown in Figure 3. For these spectra, $t_1$ was set to 17 $\mu$s which maximized the ±20 kHz regions. The notable features were a small central intensity and no new features appearing as the delay time increased. Other spectra with different $t_1$'s (not shown), though different in form, shared these characteristics. Solid-echo spectra with large echo delays ($T_2$ spectra, not shown) also had decreased central intensity.[48]

Some example 2D-X PMPS spectra are shown in Figure 4. These spectra were scaled so that the maxima at 20 kHz had approximately equal heights. Figure 5 shows the contour plots of the entire matrix of 2D-X PMPS spectra that were used in our analysis. Spectra below 50 °C (not shown) had no exchange with the $t_m$'s that were used (0.5−300 ms). The spectra in both of these figures were essentially fully relaxed and not symmetrized. The small asymmetric intensity near the

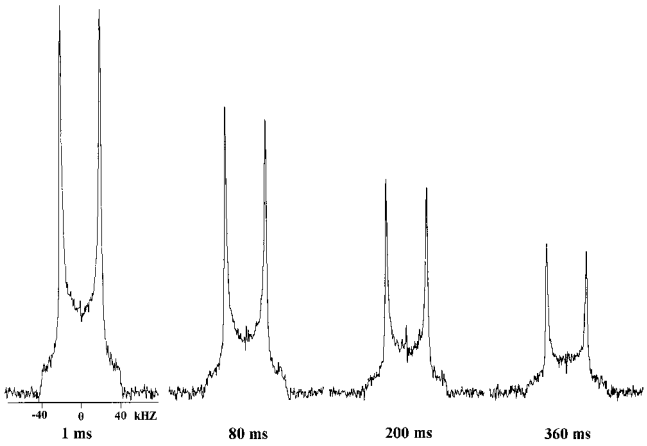


**Figure 3.** Spin alignment, $T_{1Q}$, spectra of PMPS-$d_3$ at 56 °C as a function of $t_m$. The evolution time, $t_1$, was set to 17 $\mu$s.

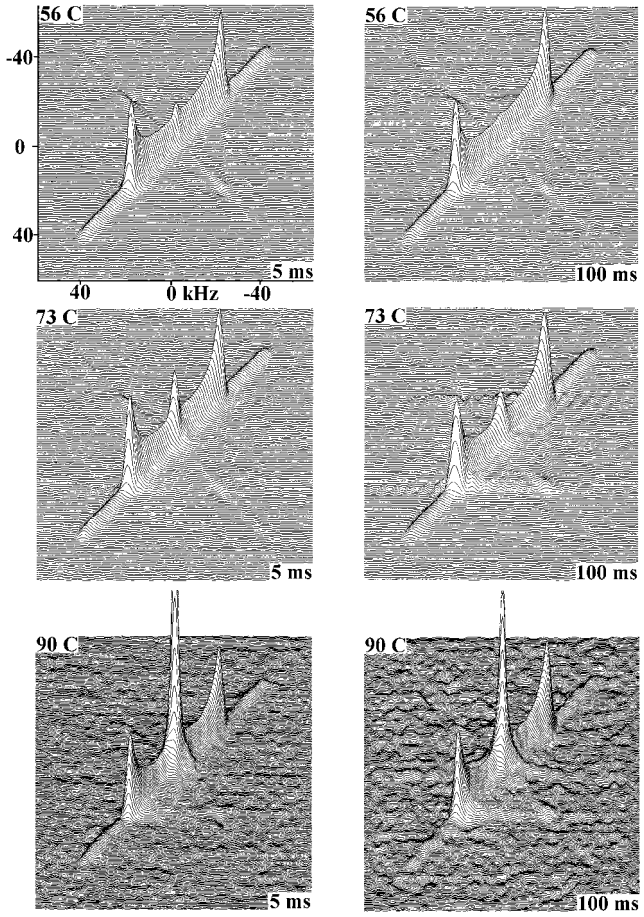


**Figure 4.** Fully relaxed $^2$H 2D-X spectra of PMPS-$d_3$ with various $t_m$'s and temperatures.

antidiagonal, most visible in the 56 °C contour plots, was common to all the spectra. The asymmetry was antisymmetric with respect to both the diagonal and antidiagonal and seemed to be the result of small imaginary signals in the time-domain data. The general characteristics of the 2D-X spectra were that there was little departure from $C_{2v}$ symmetry; a fast-isotropic peak that decreased with increasing $t_m$ (relaxation) and increased with increasing temperature; a distinct diagonal fraction that decreased with respect to exchange intensity as either $t_m$ or temperature increased; and, exchange that increased and extended further from the diagonal with increasing $t_m$ or temperature.

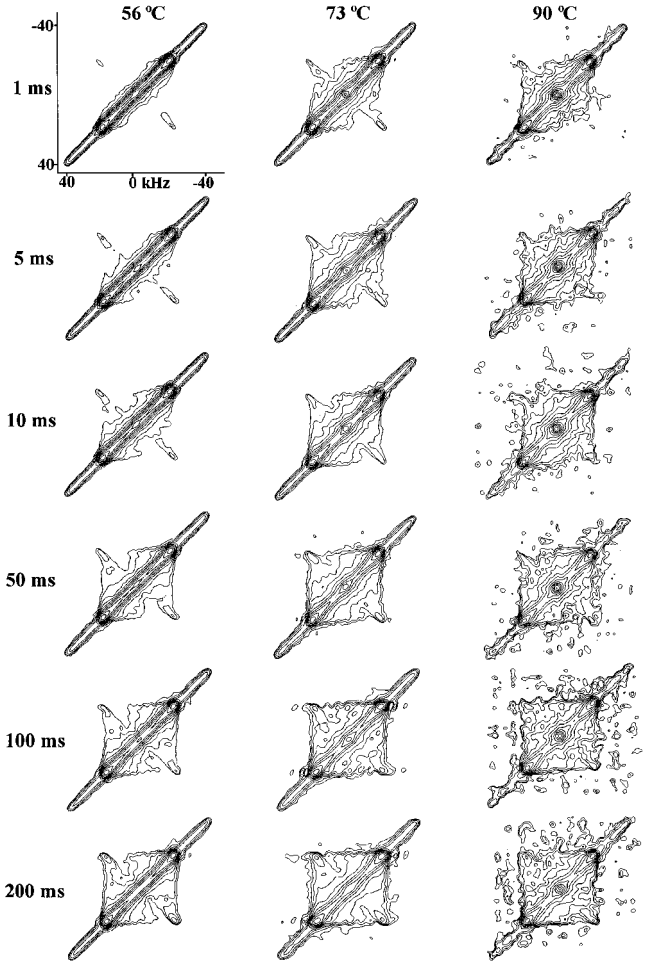


**Figure 5.** Contour plots of the experimental 2D-X spectra used in the fitting routine. Each contour level represents a 50% increase in intensity.

**Table 1. Intensity of the Diagonal Fraction with Respect to $t_m$ and Temperature[a]**

| | $t_m$ (ms) | | | | | |
|---|---|---|---|---|---|---|
| $T$ (°C) | 1 | 5 | 10 | 50 | 100 | 200 |
| 56 | 0.81 | 0.75 | 0.72 | 0.63 | 0.61 | 0.60 |
| 73 | 0.60 | 0.55 | 0.52 | 0.46 | 0.41 | 0.41 |
| 90 | 0.53 | 0.43 | 0.41 | 0.41 | 0.39 | 0.39 |

[a] The isotropic region ($\omega$ < 8 kHz) was excluded.

Another observation was that though the exchange generally increased with increasing $t_m$, the ratio of exchange to diagonal intensity remained relatively constant above some $t_m$ (about 100 ms at 73 °C). This $t_m$, denoted $t_{max}$, appeared to decrease as temperature increased. To better illustrate the $t_{max}$ behavior, the fractions of diagonal intensity in relation to $t_m$ and temperature are listed in Table 1. These fractions are the diagonal intensity divided by the diagonal plus exchange intensity; i.e., the region containing the fast-isotropic resonance was omitted in the integration.

Several distributions were used in attempts to fit the spectra. Unimodal forms of the log-normal (LN), SSLN, and SE distributions fit the spectra poorly, always converging to the broadest possible distribution. Bimodal forms of these distributions with a fast ($\tau_m < 10^{-4}$ s) and a slow ($\tau_m > 10^{-3}$ s) component reproduced the intensity losses and fast-isotropic fractions present at each temperature. However, the minimization routine could not match the slow component to the exchanging

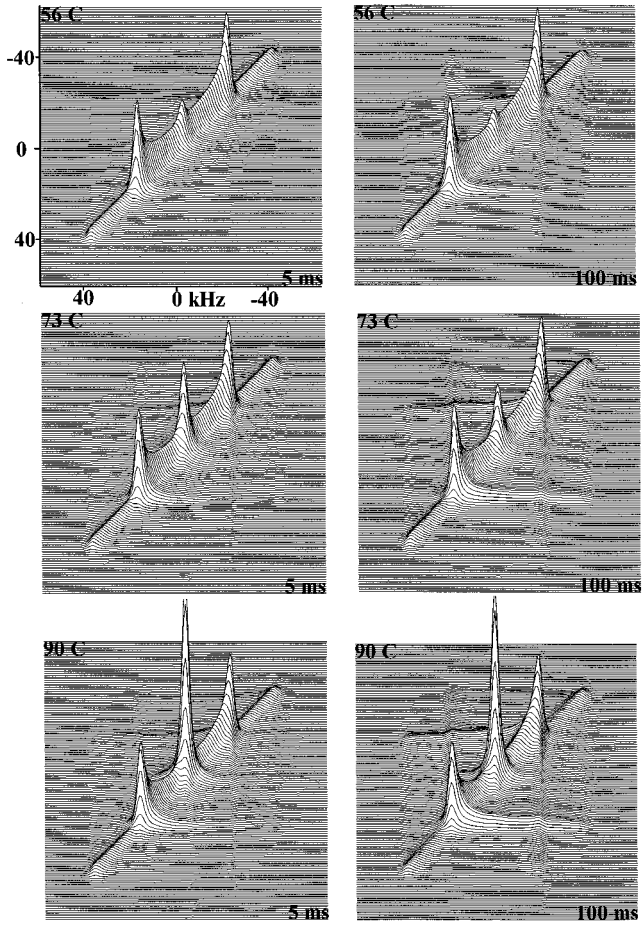


**Figure 6.** Simulated 2D-X spectra corresponding to experimental spectra of Figure 4. These simulations were based on the trimodal distributions shown in Figure 9.

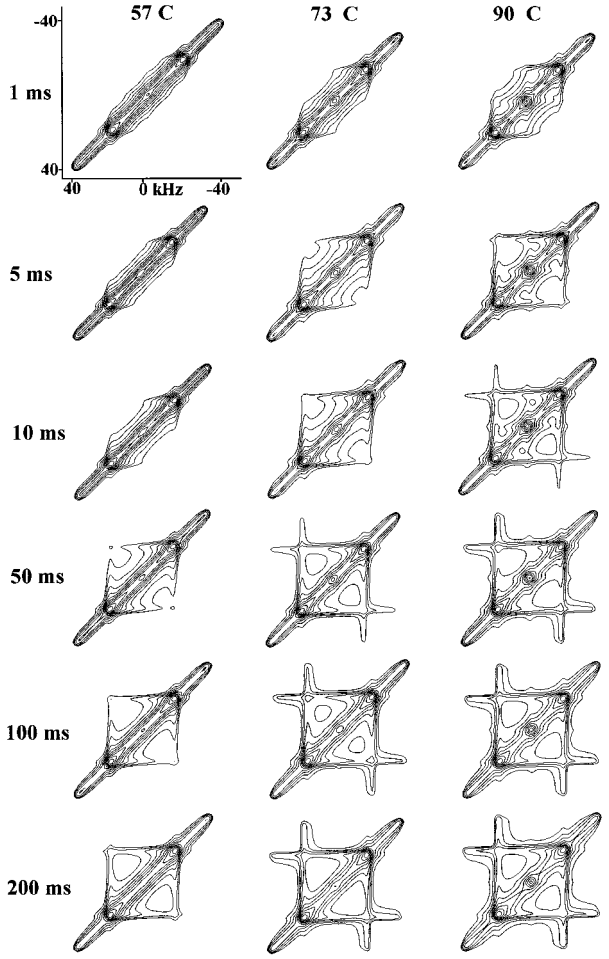


**Figure 7.** Contour plots of the simulated 2D-X spectra corresponding to experimental spectra of Figure 5. These simulations were based on the trimodal distributions shown in Figure 9. Each contour level represents a 50% increase in intensity.

and rigid ratios throughout the $t_m$ series. These fits resulted in broad distributions for the slow component and no $t_{max}$ behavior. Bimodal distributions with an exchanging ($\tau_m > 10^{-3}$ s) and a rigid ($\tau_m > 10$ s) mode did reproduce the exchange-to-rigid ratios and the $t_{max}$ behavior; but, they could not match the spectral intensity and fast-isotropic fractions.

A trimodal SE distribution was ultimately used to reproduce all the experimental data. Figures 6 and 7 show simulated spectra and contour plots, based on these fits, that correspond to the experimental spectra in Figures 4 and 5. The trimodal fits reproduced the fast-isotropic, exchanging, and rigid ratios; the spectral intensities; and the $t_{max}$ of the experimental spectra. Also, the spectral changes of the intermediate region appeared to be minimal, as they were in the experimental spectra, which supports not incorporating them into the fitting routine. Table 2 lists the parameters of the trimodal fits. Figure 8 depicts part of the calculation involved in fitting the 73 °C spectra to the distribution. It shows the actual distribution, the spectral intensity that dips in the intermediate motion regime, and the resulting observed distribution that was the product of the actual distribution and spectral intensity. The observed distribution was used to calculate the composite RAD's as discussed in the Experimental Section. Figure 9 shows the fitted trimodal distributions for the three temperatures probed. The logarithmic averages were around 40 s for the slow components, 6 $\mu$s for the fast components, and labeled on the figure for the intermediate fractions.

**Table 2. SE Trimodal Fitting Parameters for PMPS at Various Temperatures[a]**

| | | fast-isotropic | | | exchange | | | static | | |
|---|---|---|---|---|---|---|---|---|---|---|
| $T$ (°C) | $\delta^b$ | fraction | $\tau_m$ ($\mu$s) | α | fraction | $\tau_m$ (ms) | α | fraction | $\tau_m$ (s) | α |
| 56 | 41.0 | 0.21 | 10 | 0.84 | 0.24 | 240 | 0.54 | 0.55 | 82 | 0.74 |
| 73 | 40.5 | 0.35 | 9.8 | 0.81 | 0.27 | 79 | 0.42 | 0.38 | 70 | 0.47 |
| 90 | 39.5 | 0.50 | 8.9 | 0.67 | 0.18 | 21 | 0.39 | 0.32 | 85 | 0.40 |

[a] The parameters for the SE are defined in eq 4. [b] $\delta = {}^3/_4$ QCC (kHz) or the splitting between the ±20 kHz (roughly) maxima.

To some extent, the minimization routine could also be used to distinguish between the shapes of the individual modes (LN, SSLN, or SE). For the isotropic mode, the LN and SSLN resulted in fast-isotropic resonances broader than those observed in the experimental spectra. Additionally, as for the fast mode, the LN had too much intensity between $10^{-5}$ and $10^{-4}$ s (because of its symmetry) and the subsequent simulations had pronounced asymmetry. This particular fit also indicated the necessity of checking the results with $t_1-t_2$-motion sensitive simulations when the spectral changes of the intermediate region are ignored. For the exchanging mode, the LN converged to $t_m$'s approximately one-fifth of those of the SE with $t_{max}$'s about twice as long as both the SE and the apparent experimental values. These differences were also a result of the symmetry of the LN. Within experimental error,

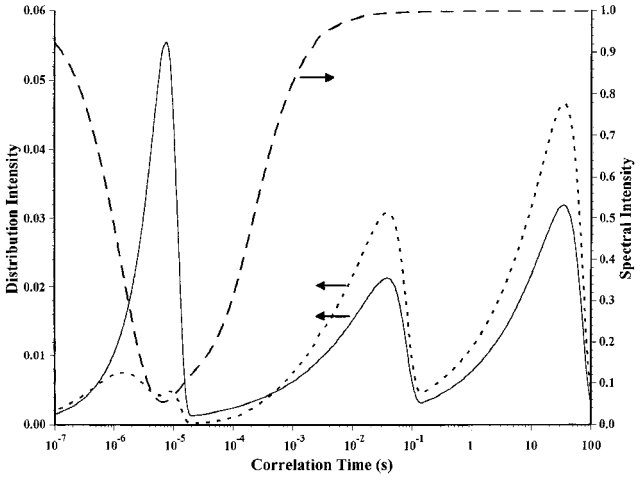


**Figure 8.** Intensity profile (– –), actual (—), and observed (···) distributions for PMPS-$d_3$ at 56 °C. The intensity is based on the solid-echo pulse sequence with a 30 $\mu$s delay.

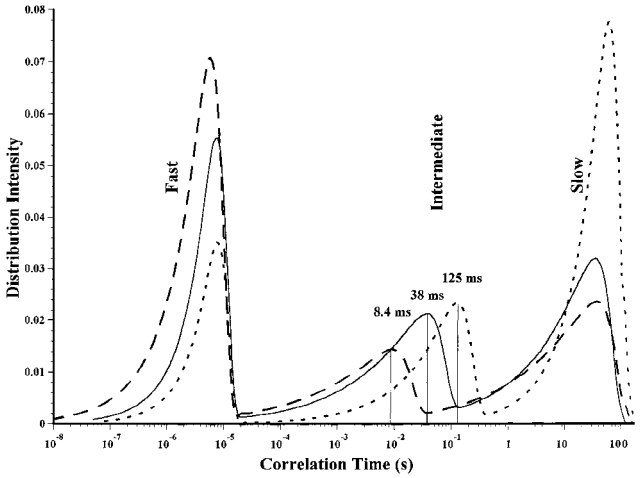


**Figure 9.** The actual 56 (···), 73 (—), and 90 °C (– –) distributions of PMPS based on the parameters in Table 2. The vertical lines in the intermediate modes represent the position of the logarithmic averages for these modes.

the SSLN fit the exchanging and rigid components as well as the SE; but, overall, the SE distribution, which was the most skewed to short $\tau_c$, fit the fast ($\tau_c < 10^{-3}$ s), exchanging ($10^{-3} < \tau_c < 1$ s), and slow ($\tau_c > 1$ s) fractions best.

The RAD's of the experimental and fit spectra at 73 °C are shown in Figure 10. Graphs from the 56 and 90 °C data were similar. As mentioned previously, these graphs show the fractions of the methyl symmetry axis that reoriented $\beta$ degrees. The experimental RAD's were generated from unconstrained, free fits of subspectra to the spectra, and the constrained RAD's were calculated from the IRD distribution model that was fit to the spectra. Both procedures were described in the Experimental Section. Along with quantifying the angles of reorientation, the similarity of the RAD's showed the ability of the constrained fitting routine to fit the slow-motion aspects of the spectra, even with the low S/N ratio of our spectra.

Finally, the morphology and bulk thermal characteristics of our sample were checked with X-ray and DSC. The powder X-ray diffraction pattern (not shown) was similar to others published.[10] It showed that our PMPS-$d_3$ sample was primarily amorphous. The only sharp peak was around 10 Å, which was supposedly the interchain distance.[10] Unlike previously published results,[13] the DSC thermogram, Figure 11, showed a broad endothermic transition between 40 and 105 °C, which was marked by a large maxima at 55 °C and a smaller one at 96 °C. This broad transition may have been preceded by a $T_g$-like transition between 5 and 30 °C. These transitions were present with both heating and cooling programs of the DSC and did not appear to be dependent on the thermal history. The only annealing effect observed was a small increase in the shoulder before the 55 °C maxima after the sample was at ambient temperatures for days. No other transitions were observed from −100 to +300 °C.

## Discussion

The changes that occur to the PMPS-$d_3$ solid-echo spectra as the temperature increases are *atypical* of amorphous polymers. Because the time scale of the solid-echo experiment is around $10^{-5}$ s, the spectra of amorphous polymers usually begin to change at about 30 °C above their calormetrically determined $T_g$'s.[49] Typically, as the temperature increases to $T_g + 30$, the powder pattern of an amorphous polymer gradually loses width and intensity. Then, as the temperature further increases, it collapses into a fast-isotropic resonance and gains intensity. For example, the spectra of poly(vinyl acetate)-$d_3$ (PVAc-$d_3$, $T_g = 30°$) begin to lose width and shape at 60 °C and converge to an isotropic resonance at 82 °C.[50] Solid poly(methyl acrylate)-$d_3$ (PMA-$d_3$) and poly(α-methylstyrene)-$d_3$ (PαMS-$d_3$) are similar.[51,52] Their line shapes completely collapse about 45 °C above their calorimetric $T_g$'s of 10 and 130 °C, respectively. Unlike PVAc-$d_3$, PMA-$d_3$, and PαMS-$d_3$, the solid-echo spectra of PMPS-$d_3$ change nearly coincident with its DSC transition. The rigid line shape does not gradually collapse as temperature increases, either. Instead, the intensity shifts from the rigid powder spectrum to the fast-isotropic resonance. The small reduced splitting that does occur is likely the result of small angle (<5°) librations.[53,54]

For the polymers mentioned above and many others,[24] the line-shape changes above $T_g$ correspond well with segmental motion that is isotropic and diffusive in nature. Generally, this motion has a distribution of rates and may be accompanied by large angle jump[21] or restricted by bulky side groups.[20,39,53,54] The dynamics of PMPS-$d_3$ also appear to be diffusive. As shown by Hirschinger et al.,[55,56] both the lack of additional maxima in the $T_{1Q}$ spectra as $t_m$ increases and the decreased intensities in the centers of the $T_{1Q}$ and $T_2$ spectra are consistent with IRD. In the 2D-X spectra, the gradual spreading of exchange into the 2D plane as $t_m$ increases and the lack of elliptical patterns support IRD and eliminate random jumps, large angle jumps, and specific jumps.[24] Thus, IRD seems reasonable as a first approximation to describe the mechanism of segmental dynamics in PMPS-$d_3$, but a combination of mechanisms is not eliminated.[21]

The distribution of $\tau_c$'s appears to be the main cause of the unusual spectral behavior of PMPS-$d_3$. Typically, the segmental motion of amorphous polymers is characterized with a broad, unimodal, and heterogeneous distribution of $\tau_c$'s that gradually shifts toward faster times as temperature increases. The superposition of fast-isotropic and rigid components in the PMPS-$d_3$ spectra does confirm a heterogeneous distribution of $\tau_c$'s,[44] but neither the solid-echo nor the 2D-X spectra

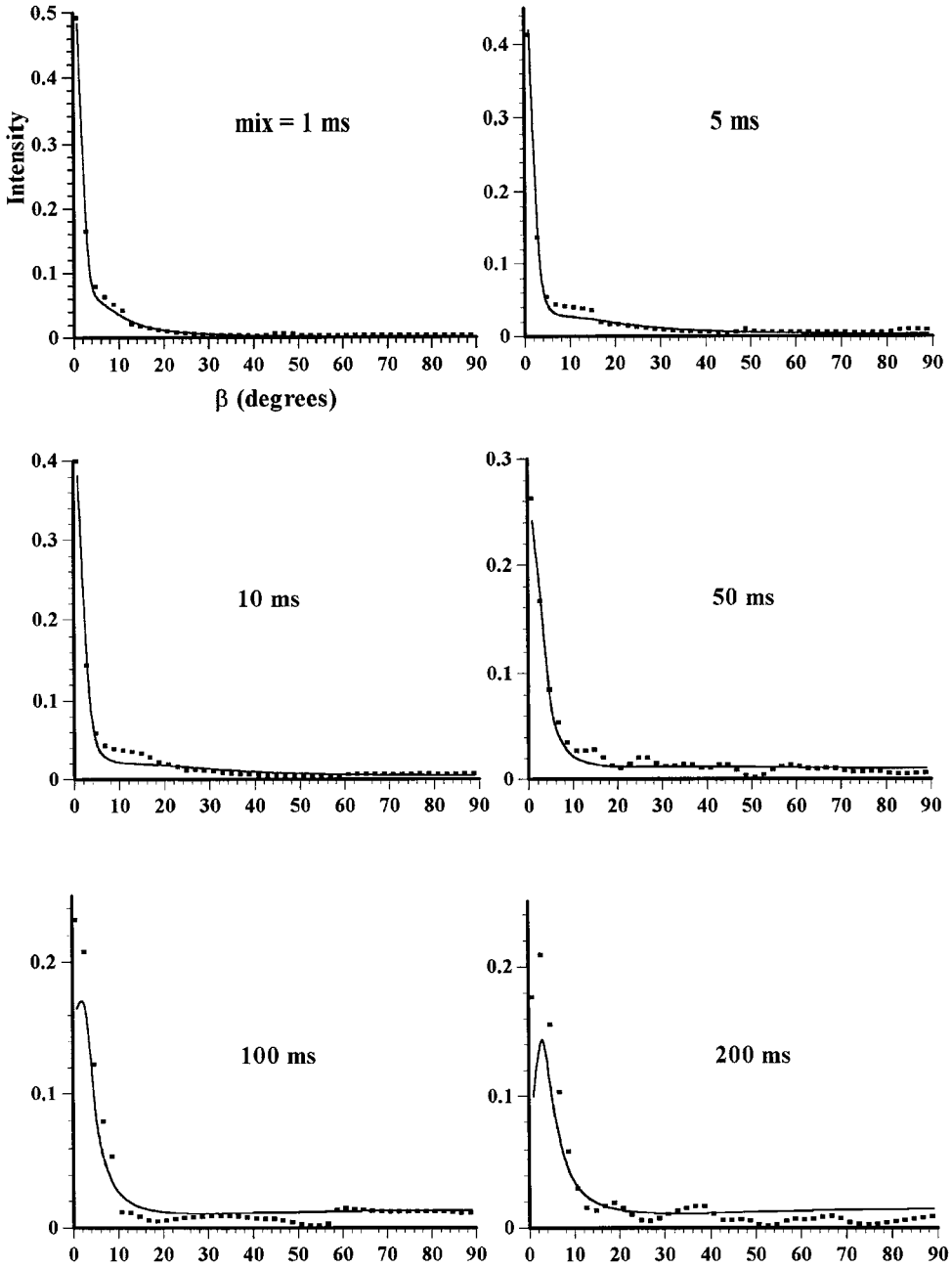


**Figure 10.** RAD's from the unconstrained fit of the 73 °C experimental spectra (···) and from the fit constrained to the IRD model with a distribution of $\tau_c$'s (—).

are consistent with the typical distribution. Solid-echo and 2D-X simulations (not shown) based on IRD and a reduced QCC = 170/3 kHz show that the most dramatic deviations from either a static or fast-isotropic line shape or from $C_{2v}$ symmetry in 2D-X spectra occur with $\tau_c$'s between $10^{-3.5}$ and $10^{-4.5}$ s. These simulations also show that the greatest intensity reduction occurs with $\tau_c$'s around $10^{-5}$ s and that the fast-isotropic peak is from species with $\tau_c$'s below $10^{-5.7}$ s. Together, the rigid powder pattern, intensity reduction, $C_{2v}$ symmetry of the 2D-X spectra, and fast-isotropic peak are consistent with segmental motion with $\tau_c$'s above $10^{-3}$ s (rigid) and below $10^{-4.5}$ s (fast-isotropic and lost intensity), but with little motion between (line-shape changes and asymmetry). Additionally, in the 2D-X spectra below 50 °C, the lack of exchange further constrains the slow fraction to $\tau_c$'s on the order of seconds. Thus, from 10 to 50 °C, the data are consistent with a bimodal distribution with $\tau_c$'s below $10^{-4.5}$ and above 10 s (approximately). And, as the temperature increases, the intensity shifts from the rigid to the mobile fraction, but the time scales of the two fractions remain relatively constant.

To account for the exchange and diagonal above 50 °C, the distribution that characterizes the slow fraction must have an intensity around 1 ms and above 20 s (roughly 100 times the longest $t_m$). Furthermore, the small amount of exchange and prominent diagonal suggest that the distribution has its primary intensity around 20 s and is skewed toward 1 ms, similar to the SE and SSLN distributions. With such distributions, the exchange increases with increasing $t_m$ as occurs in PVAc, PMA, PαMS, and simulations based on fits to the PMPS-$d_3$ spectra from such distributions. However, in the experimental PMPS-$d_3$ spectra, exchange stops increasing after $t_{max}$. A fraction of polymer that is completely exchanged around $t_{max}$ could account for both the diagonal and exchange in the PMPS-$d_3$ spectra.[57] Poly(methyl methacrylate) and poly(ethyl methacry-

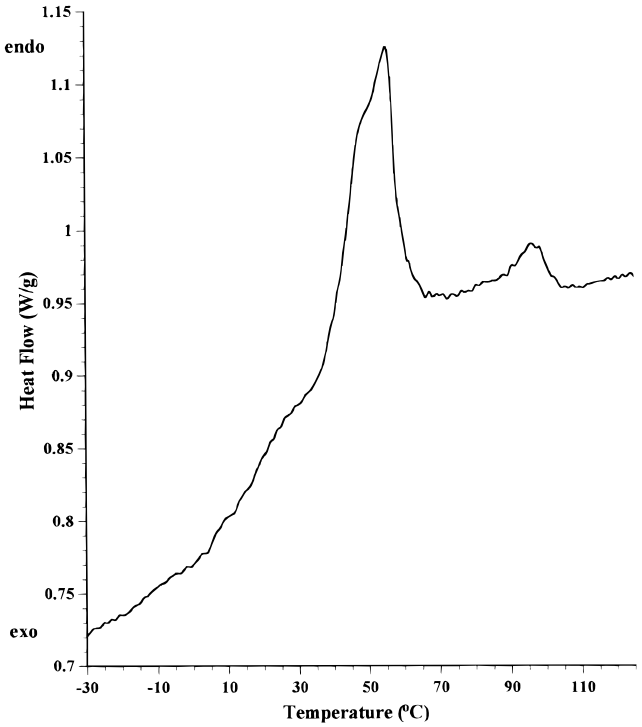


**Figure 11.** DSC thermogram of PMPS-$d_3$ at a scan rate of 3 °C/min.

late), where some side groups remain rigid and some reorient, have similar 2D-X spectra.[20,39] Such situations are also known for polymer blends.[58,59] For PMPS-$d_3$, the combination of a rigid and exchanging fraction, along with the mobile fraction (fast-isotropic and lost intensity), leads to a *trimodal* distribution. As already mentioned, the fits from a trimodal SE distribution and their subsequent simulations reproduce all the characteristics of the experimental spectra. Table 2 and Figure 9 show the parameters and forms of the distributions, respectively, for the temperatures probed. As expected, the exchanging fractions shift to smaller $\tau_c$'s as temperature increases, reproducing the trend in $t_{max}$.

A trimodal distribution in a chemically homogeneous, glassy polymer is unusual, although multimodal distributions have been observed in polymer blends and for diluents in polymers.[58−60] For these systems, the different modes were attributed to either intrinsic dynamic differences between the species, variations in the local composition, or both. For PMPS, the different tacticities could have different segmental dynamics. However, the different methyl environments should also have different $T_1$'s and we found the $T_1$'s of the exchanging and rigid fractions to be roughly equal.[57] For an amorphous homopolymer, local compositional changes would be manifested as density or packing fluctuations. Such fluctuations are common to polymers and, though perhaps responsible for the distribution in general, they do not usually cause multimodal distributions. Thus, without added complications, these possibilities are not the likely cause for the shifting of intensity as temperature changes.

Semicrystalline polymers can be described as being composed of amorphous, interphase, and crystalline regions.[61] Some crystallinity exists in PMPS-$d_3$; so, it seems reasonable to assign the fast fraction to the amorphous regions, the rigid fraction to the crystalline regions, and the exchanging fraction to the interphase between the two. With this explanation, the intensity shifts from rigid to fast-isotropic because the polymer melts and becomes amorphous. A surface-melting process would even be consistent with the relatively constant fraction of interphase.[62] A nearly identical situation was observed with Raman spectroscopy in polyethylene (PE).[63] NMR studies on PE[64−66] and poly(butylene terephthalate)[30] were similarly interpreted in terms of three components. Both the DSC endotherms and the NMR data of PMPS-$d_3$ coincide well with a semicrystalline morphology. Unfortunately, the X-ray diffraction pattern of our PMPS-$d_3$ sample is much more typical of an amorphous polymer than a semicrystalline one (less than 5% crystallinity). And, it certainly does not support the degree of crystallinity that the rigid fraction implies. Our PMPS-$d_3$ sample could, however, have a high degree of local order and little long-range or macroscopic order. The 10 Å peak in the diffractogram, which is roughly 30% of the total intensity, is consistent with such a suggestion, as is a recent extensive X-ray study.[67] DSC thermograms and solid-echo spectra of liquid-crystalline polymers are also similar to the PMPS-$d_3$ data, suggesting a microscopically ordered phase.[68]

Aside from the meltlike transition to fast $\tau_c$'s above 50 °C, which both the NMR and DSC data support, it seems reasonable to suppose that the initial (below 50 °C) intensity loss and fast-isotropic resonance are the result of a separate mobile fraction, perhaps composed of lower molecular weight polymer, chain ends, etc. To be consistent with the 56 °C data, this fraction would probably comprise about 20% of the polymer. We could not verify the existence of such a fraction, though. 2D-X spectra from 0 to 50 °C are diagonal at $t_m$'s from 0.5 to 300 ms, and the solid-echo spectra from −125 to 50 °C are essentially identical in shape except for the fast-isotropic resonance and intensity loss above 25 °C. Thus, we could not observe such a fraction gradually moving to faster $\tau_c$'s with increasing temperature. We are left with the conclusion that either this fraction has a very broad distribution (3−4 orders of magnitude), which might have eluded detection, or that different segments undergo meltlike transitions at different temperatures.

## Conclusions

Our method for fitting experimental 2D-X spectra seems robust and, within the framework of a model, does consistently quantify spectra. Below 50 °C, we observe two fractions in solid-state PMPS-$d_3$—a fast fraction with $\tau_c$'s generally below $10^{-5}$ s and one with $\tau_c$'s above 10 s. Above 50 °C, the spectra are consistent with the model of IRD with a trimodal stretched-exponential distribution of $\tau_c$'s. The distribution has a fast ($10^{-7} < \tau_c < 10^{-5}$ s), intermediate ($10^{-4} < \tau_c < 0.4$ s), and rigid (10 s $< \tau_c$) mode. As the temperature increases from 56 to 90 °C, the distribution of each fraction broadens, the fast fraction increases from 21% to 50% while its average $\tau_c$ remains roughly constant at $10^{-5}$ s, the amount of the intermediate fraction remains relatively constant at 23% while its average $\tau_c$ decreases from 125 to 8 ms, and the rigid fraction decreases from 55% to 32% with an average $\tau_c$ around 40 s. The continual shifting from the rigid to the fast region as the temperature increases is indicative of melting, but the X-ray diffractogram shows very little crystallinity. The diffractogram is, however, consistent with a substantial amount of local order. We attribute

the fast fraction to amorphous, melt-like polymer, the rigid fraction to crystalline-like polymer, and the intermediate fraction to an interphase between the two. In contrast to both amorphous and semicrystalline systems, PMPS-$d_3$ may have a substantial amount of local order, but very little long-range, macroscopic order.

**Acknowledgment.** The authors wish to thank the National Science Foundation under grant DMR9500926 and IBM for financial support of the project.

## References and Notes

(1) Trujillo, R. E. *J. Organomet. Chem*. **1980**, *198*, 27.
(2) Miller, R. D.; Michl, J. *Chem. Rev*. **1989**, *89*, 1359.
(3) Miller, R. D. *Adv. Mater*. **1989**, *12*, 433.
(4) Kajzar. F.; Messier. J.; Rosilio, C. *J. Appl. Phys*. **1986**, *60*, 3040.
(5) Fujii, A.; Yoshimoto, K.; Yoshida, M.; Ohmori, Y.; Yoshino, K. *Jpn. J. Appl. Phys., Part 2 Lett*. **1995**, *34*, 1365.
(6) Suzuki, H.; Meyer, H.; Hoshino, S.; Harrer, D. *J. Appl. Phys*. **1995**, *78*, 2684.
(7) Abkowitz, M.; Stolka, M. *Philos. Mag. Lett*. **1988**, *58*, 239.
(8) Wolf, A. R.; West, R. *Appl. Organomet. Chem*. **1987**, *1*, 7.
(9) Demoustier-Champagne, S.; de Mahieu, A.-F.; Devaux, J.; Fayt, R.; Teyssie, Ph. *J. Polym. Sci., Polym. Chem. Ed*. **1993**, *31*, 2009.
(10) Maxka, J. Ph.D. Dissertation, University of Wisconsin, Madison, 1988.
(11) Maxka, J.; Mitter, F. K.; Powell, D. R.; West, R. *Organometallics* **1991**, *10*, 660.
(12) Lacavegoffin, B.; Hevesi, L.; Devaux, J. *Chem. Commun*. **1996**, *6*, 765.
(13) Demoustier-Champagne, S.; Devaux, C.; Devaux, J. *Polymer* **1995**, *36*, 1003.
(14) Welsh, W. J.; Damewood, J. R., Jr.; West, R. C. *Macromolecules* **1989**, *22*, 2947.
(15) Garbassi, F.; Morra, M.; Occhiello, E. *Polymer Surfaces;* John Wiley & Sons: Chichester, U.K., 1995.
(16) Ferry, J. D. *Viscoelastic Properties of Polymers*; Wiley: New York, 1980.
(17) Robyr, P.; Tomaselli, M.; Grob-Pisano, C.; Meier, B. H.; Ernst, R. R.; Suter, U. W. *Macromolecules* **1995**, *28*, 5320.
(18) Brown, H. R. *Science* **1993**, *263*, 1411.
(19) Newby, B. Z.; Chaudhury, M. K.; Brown, H. R. *Science* **1994**, *269*, 1407.
(20) Kulik, A. S.; Beckham, H. W.; Schmidt-Rohr, K.; Radloff, D.; Pawelzik, U.; Boeffel, C.; Spiess, H. W. *Macromolecules* **1994**, *27*, 4746.
(21) Leisen, J.; Schmidt-Rohr, K.; Spiess, H. W. *J. Non-Cryst. Solids* **1994**, *172*−*174*, 737.
(22) Fytas, G.; Meier G.; Dorfmüller, Th.; Patkowski, A. *Macromolecules* **1982**, *15*, 214.
(23) Abragam, A. *Principles of Nuclear Magnetism*; Oxford University Press: Oxford, U.K., 1961.
(24) Schmidt-Rohr, K.; Spiess, H. W. *Multidimensional Solid-State NMR and Polymers*; Academic Press Limited: London, 1994.
(25) Spiess, H. W. *Annu. Rev. Mater. Sci*. **1991**, *21*, 131.
(26) Jelinski, L. W. *Annu. Rev. Mater. Sci*. **1985**, *15*, 359.
(27) naNagara, B.; O'Connor, R. D.; Blum, F. D. *J. Phys. Chem*. **1992**, *96*, 6417.
(28) Schleicher, A.; Müller, K.; Kothe, G. *J. Chem. Phys*. **1990**, *92*, 6432.
(29) Lee, P. L.; Schaefer, J. *Macromolecules* **1995**, *28*, 1921.
(30) Schmidt-Rohr, K.; Spiess, H. W. *Macromolecules* **1991**, *24*, 5288.
(31) Kaufmann, S.; Wefing, S.; Schaefer, D.; Spiess, H. W. *J. Chem. Phys*. **1990**, *93*, 197.
(32) Wefing, S.; Kaufmann, S.; Spiess, H. W. *J. Chem. Phys*. **1988**, *89*, 1234.
(33) Wefing, S.; Spiess, H. W. *J. Chem. Phys*. **1988**, *89*, 1219.
(34) Schaefer, D.; Leisen, J.; Spiess, H. W. *J. Magn. Reson*. **1995**, *115*, 60.
(35) Hagemeyer, A.; Brombacher, L.; Schimdt-Rohr, K.; Spiess, H. W. *Chem. Phys. Lett*. **1990**, *167*, 583.
(36) Schaefer, D.; Spiess, H. W. *J. Chem. Phys*. **1992**, *97*, 7944.
(37) Schmidt, C.; Kuhn, K. J.; Spiess, H. W. *Prog. Colloid Polym. Sci*. **1985**, *71*, 71.
(38) Leisen, J.; Schmidt-Rohr, K.; Spiess, H. W. *Physica A* **1993**, *201*, 79.
(39) Schmidt-Rohr, K.; Kulik, A. S.; Beckham, H. W.; Ohlemacher, A.; Pawelzik, U.; Boeffel, C.; Spiess, H. W. *Macromolecules* **1994**, *27*, 4733.
(40) Schmidbaur, H. *Chem. Ber*. **1991**, *124*, 1953.
(41) Jones, R. G.; Benfield, R. E.; Cragg, R. H.; Swain, A. C. *J. Chem. Soc., Chem. Commun*. **1992**, 112.
(42) Davis, J. H.; Jeffrey, K. D.; Bloom, M.; Valic, M. F.; Higgs, T. P. *Chem. Phys. Lett*. **1976**, *42*, 390.
(43) Schmidt, C.; Blümich, B.; Spiess, H. W. *J. Magn. Reson*. **1988**, *79*, 269.
(44) Kaplan, J. I.; Garroway, A. N. *J. Magn. Reson*. **1982**, *49*, 464.
(45) Bendler, J. T.; Shlesinger, M. F. In *Studies in Statistical Mechanics*; Shlesinger, M. F., Weiss, G. H., Eds.; North-Holland: New York, 1985; Vol. 12.
(46) Marquardt, D. *SIAM J. Appl. Math*. **1963**, *11*, 431. FORTRAN IMSL routine BCLSJ. In the program, both the mechanism (IRD) and distribution can be changed.
(47) The error for a spectrum was calculated as:

$$\text{error} = \sqrt{\sum_{i=1}^{n}\left(\frac{\text{th}_i - S_i}{S_i}\right)^2 / n}$$

where $n$ is the number of points, $\text{th}_i$ is the theoretical value for point $i$, and $S_i$ is the experimental spectrum's corresponding value. Generally, the omitted points greater than 2 standard deviations, which we defined as the square of the error, from the average error were from experimental points 1 order of magnitude different from their neighbors and obviously noise.
(48) O'Connor, R. D.; Blum, F. D.; Ginsburg, E.; Miller, R. D. *Polym. Prepr*. **1994**, *35*, 417.
(49) McCall, D. C. *Acc. Chem. Res*. **1971**, *4*, 223.
(50) Blum, F. D.; Xu, G.; Liang, M.; Wade, C. G. *Macromolecules* **1996**, *29*, 8740.
(51) Lin, W. Y.; Blum, F. D. *Macromolecules* **1997**, *30*, 5331.
(52) O'Connor, R. D.; Blum, F. D.; Ginsburg, E.; Miller, R. D. To be submitted.
(53) Kulik, A. S.; Radloff, D.; Spiess, H. W. *Macromolecules* **1994**, *27*, 3111.
(54) Kuebler, S. C.; Heuer, A.; Spiess, H. W. *Macromolecules* **1996**, *29*, 7089.
(55) Hirschinger, J.; English, A. D. *J. Magn. Reson*. **1989**, *85*, 542.
(56) Hirschinger, J.; Miura, H.; Gardner, K. H.; English, A. D. *Macromolecules* **1990**, *23*, 2153.
(57) It is unlikely that relaxation effects are the cause of the $t_{max}$ behavior. For relaxation to cause the $t_{max}$ behavior, the $T_1$'s for the exchanging fractions would need to be on the order of $t_{max}$ or approximately 100 ms at 73 °C and 20 ms at 90 °C. At these temperatures, differences should be noticeable in the rigid-to-exchange ratios of partially relaxed spectra compared to fully relaxed spectra. However, partially relaxed spectra of PMPS-$d_3$ (not shown) with relaxation delays of 0.3 s, which is one $T_1$ for the rigid and 3−10 $T_1$'s for the exchange, were essentially identical in their exchange-to-rigid ratios to the fully relaxed spectra. Also, a $T_1$ of 20 ms would be physically unreasonable.
(58) Chung, G.-C.; Kornfield, J. A.; Smith, S. D. *Macromolecules* **1994**, *27*, 964.
(59) Chin, Y. H.; Inglefield, P. T.; Jones, A. A. *Macromolecules* **1993**, *26*, 5372.
(60) Zhang, C.; Wang, P.; Jones, A. A.; Inglefield, P. T.; Kambour, R. P. *Macromolcules* **1991**, *24*, 338.
(61) Flory, P.; Yoon, D. Y.; Dill, K. A. *Macromolecules* **1984**, *17*, 862.
(62) Stroble, G. *The Physics of Polymers*; Springer-Verlag: Berlin, 1996.
(63) Mutter, R.; Stille, W.; Strobl, G. *J. Polym. Sci., Phys. Ed*. **1993**, *31*, 99.
(64) Cholli, A. L.; Dumais, J. J.; Engel, A. K.; Jelinski, L. W. *Macromolecules* **1984**, *17*, 2399.
(65) Horii, F.; Kitamaru, R. *J. Polym. Sci., Polym. Phys. Ed*. **1978**, *16*, 265.
(66) Kitamaru, R.; Horii, F.; Hyon, S.-H. *J. Polym. Sci., Polym. Phys. Ed*. **1977**, *15*, 821.
(67) Demoustier-Champagne, S.; Jonas, A.; Devaux, J. *J. Polym. Sci. B* **1997**, *35*, 1727.
(68) Martin, Andreas; Tefehne, Christoph; Gronski, Wolfram. *Macromol. Rapid Commun*. **1996**, *17*, 305.

MA980149J